Proceedings of the
Annual Stability Conference
Structural Stability Research Council
Orlando, Florida, April 12-15, 2016

Constrained finite element method for the modal analysis of thin-walled members with holes

Sándor Ádány[1]

Abstract
In this paper a new method for modal decomposition of thin-walled members is presented. The method is based on the finite element method, by using a specific shell finite element. The specific finite element makes it possible to perform modal decomposition essentially identically as in the constrained finite strip method. The method, therefore, can be termed as constrained finite element method. In the paper the method is briefly presented, then its applicability is demonstrated. Since one of the practically useful feature of the method that it can easily handle holes, there is a special focus of the demonstrative examples on members with holes.

1. Introduction

Thin-walled members possess complicated behavior. In many cases the complex behavior can be characterized as the interaction of various simpler phenomena. This is the reason why the deformations of a thin-walled beam or column member are frequently categorized into simpler, yet practically meaningful deformation classes: global (G), distortional (D), local-plate (L) and other modes, based on some characteristic features of the deformations. Although in practical situations these modes rarely appear in isolation, the GDL classification has still been found useful for capacity prediction, and appears either implicitly or explicitly in current thin-walled design standards, too.

For critical load calculation of thin-walled beams or columns the constrained finite strip method (cFSM) is a potential tool, see Ádány and Schafer (2008) or Ádány and Schafer (2014a,b). It is based on the semi-analytical FSM (Cheung 1976, Hancock 1978), but carefully defined constraints are applied which can enforce the member to deform in accordance with a desired deformation, e.g. to buckle in flexural, lateral-torsional, or distortional mode. Another popular method that is able perform modal decomposition is the generalized beam theory (GBT), see e.g. Silvestre et al. (2011). Though these methods are useful tools, they have limitations. One such limitation is that they cannot handle members with holes. Though various attempts have been made recently to extend FSM GBT or FEM for members with holes, see e.g. Eccher et al. (2009), Casafont et al. (2011), Cai and Moen (2015), Casafont et al. (2015), a general solution for members with holes is not yet proposed.

[1] Associate Professor, Budapest University of Technology and Economics, <sadany@epito.bme.hu>

In this paper a new method is proposed. The new method uses the idea of cFSM, however, the constraining procedure is applied for shell finite elements. Since shell finite element method (FEM) can handle almost any practical problem in the realm of thin-walled members, the proposed constrained finite element method (cFEM) can provide a solid platform to handle previously unresolved problems, such as the modal decomposition of members with holes, members with cross-section changes, and so on.

The aim of this paper is to briefly present the cFEM, and demonstrate its applicability. Since one of the practically useful novel feature of cFEM is its ability to handle members with holes, the demonstrative examples will have a special focus on thin-walled beams with holes of various sizes and arrangements.

2. From cFSM to cFEM

2.1 FSM and cFSM basics

The finite strip method (FSM) can be regarded as a special version of finite element method (FEM) in which special "finite element"-s are used. The most essential feature of FSM is that there are two pre-defined directions, and the base functions (or: interpolation functions) are different in the two directions. In classical semi-analytical FSM, as in Cheung (1976) or Hancock (1978), the structural member to be analysed is discretized only in one direction (say: transverse direction), while in the other direction (say: longitudinal direction) there is no discretization, i.e., in this direction there is only one element (i.e., strip) along the member.

In a strip it is typical to express the displacement functions as a product of transverse and longitudinal base functions. In the transverse directions polynomials are used, while in the longitudinal direction trigonometric functions can beneficially be used. Since there is no longitudinal discretization, the longitudinal interpolation function must well represent the behaviour, and especially, must satisfy the boundary conditions. If the end restraints are pinned, the widely used FSM displacement functions are as follows (with using the notations of Fig 1):

$$u(x,y) = \left[\left(1-\frac{y}{b}\right) \quad \left(\frac{y}{b}\right)\right]\begin{bmatrix}u_1\\u_2\end{bmatrix} cos\frac{m\pi x}{a} \tag{1}$$

$$v(x,y) = \left[\left(1-\frac{y}{b}\right) \quad \left(\frac{y}{b}\right)\right]\begin{bmatrix}v_1\\v_2\end{bmatrix} sin\frac{m\pi x}{a} \tag{2}$$

$$w(x,y) = \left[\left(1-\frac{3y^2}{b^2}+\frac{2y^3}{b^3}\right) \quad \left(-x+\frac{2y^2}{b}-\frac{x^3}{b^2}\right) \quad \left(\frac{3y^2}{b^2}-\frac{2y^3}{b^3}\right) \quad \left(\frac{y^2}{b}-\frac{y^3}{b^2}\right)\right]\begin{bmatrix}w_1\\\Theta_1\\w_2\\\Theta_2\end{bmatrix} sin\frac{m\pi x}{a} \tag{3}$$

Other end restraints can also be handled by more complicated longitudinal base functions, e.g., expressed by trigonometric series, see Li and Schafer (2009) or Li and Schafer (2010).

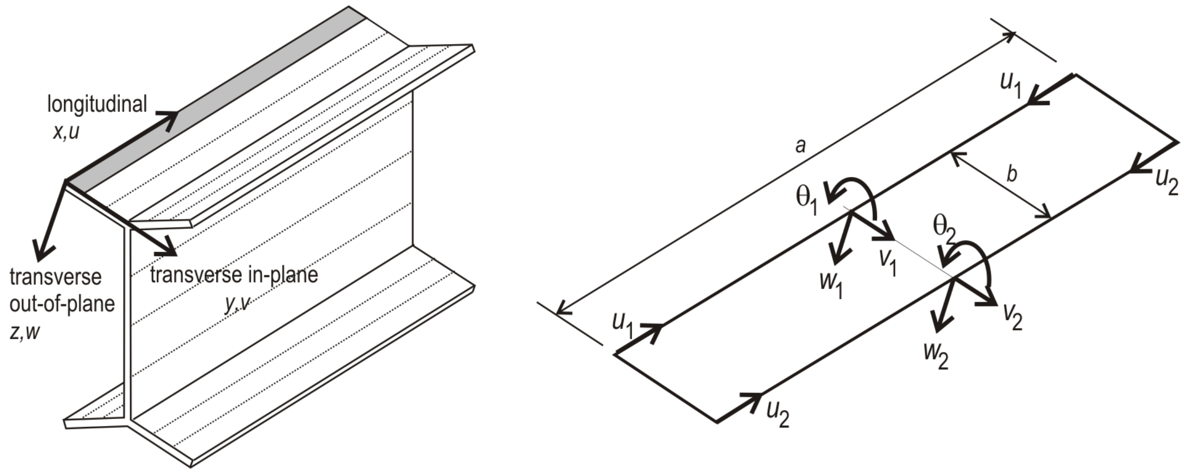

Figure 1: FSM discretization and DOF for pinned-pinned end restraints

If FSM is intended to apply to solve linear buckling problems (to get critical loads and buckling shapes), we need to construct first the local elastic and geometric stiffness matrices by following conventional FEM steps, by considering the 2D generalized Hooke's law (for the elastic stiffness matrix) and by considering the second-order strain terms (for the geometric stiffness matrix). The stiffness matrices can be determined analytically. From the local stiffness matrices the member's (global) stiffness matrices (elastic and geometric, $\mathbf{K_e}$ and $\mathbf{K_g}$) can be compiled as in FEM, by transformation to global coordinates and assembly.

For a given distribution of edge tractions on a member the geometric stiffness matrix scales linearly, resulting in the classic eigen-buckling problem, namely

$$\mathbf{K_e}\mathbf{\Phi} - \mathbf{\Lambda}\mathbf{K_g}\mathbf{\Phi} = \mathbf{0} \tag{4}$$

with

$$\mathbf{\Lambda} = \mathrm{diag} < \lambda_1\ \lambda_2\ \lambda_3\ ...\ \lambda_{nDOF} > \qquad \text{and} \quad \mathbf{\Phi} = [\boldsymbol{\phi}_\mathbf{1}\ \boldsymbol{\phi}_\mathbf{2}\ \boldsymbol{\phi}_\mathbf{3}\ ...\ \boldsymbol{\phi}_{\boldsymbol{nDOF}}] \tag{5}$$

where λ_i is the critical load multiplier and $\boldsymbol{\phi}_{\boldsymbol{i}}$ is the associated buckling shape, and *nDOF* denotes the number of degrees of freedom.

The constrained FSM (cFSM) is a special version of FSM that uses mechanical assumptions to enforce or classify deformations to be consistent with a desired set of criteria. The method is originally presented in Ádány and Schafer (2006a,b) and Ádány and Schafer (2008). The cFSM constraints are mechanically defined, and are utilized to formally categorize deformations into global (G), distortional (D), local (L), and other (i.e., shear and transverse extension, S+T) deformations. Once the mechanical criteria are transformed into constraint matrices, any FSM displacement field $\mathbf{d}$ (e.g. an eigen-buckling mode $\boldsymbol{\phi}$ is an important special case) may be constrained to any modal $\mathbf{d_M}$ deformation space via:

$$\mathbf{d} = \mathbf{R_M}\mathbf{d_M} \tag{6}$$

where $\mathbf{R_M}$ is a constraint matrix, the derivation of which can be found in Ádány and Schafer (2014a,b) for general cross-sections, and M might be G, D, L, S and/or T.

Though modal decomposition is not restricted to eigen-buckling solution, this is the problem where modal decomposition is mostly used. It can be completed by applying $\mathbf{R_M}$ for the intended space (M = G, D, L, S, and/or T). Eq. (4) becomes:

$$\mathbf{R_M}^{\mathrm{T}}\mathbf{K_e}\mathbf{R_M}\mathbf{\Phi_M} - \mathbf{\Lambda}\mathbf{R_M}^{\mathrm{T}}\mathbf{K_g}\mathbf{R_M}\mathbf{\Phi_M} = \mathbf{0} \tag{7}$$

which is another generalized eigen-value problem, given in the reduced M deformation space.

The constraint matrices are based on the mechanical criteria characteristics for the deformation mode. The criteria are given in detail in Ádány and Schafer (2014a,b), expressed mostly by setting certain displacement and displacement derivatives to zero. For example, G, D and L modes are characterized by zero transverse extension and zero in-plane shear, but L modes furthermore are characterized by zero longitudinal extension. The constraint matrix enforces certain relationship in between various nodal degrees of freedom. Another view of constraint matrix is that the column vectors of the matrix are the modal base vectors of the displacement field that is represented by the constrain matrix.

2.2 Shell finite element for cFEM

The goal here is to transform the "finite strip" into a shell "finite element". Since the above-summarized semi-analytical FSM uses classic polynomials in the transverse direction, the new shell element can inherit the transverse interpolation functions from FSM. The longitudinal interpolation function should be changed, however, by keeping some important characteristics of the functions of FSM. These key features are as follows:

- they must be able to exactly satisfy the constraining criteria for mode decomposition (no-shear criterion, no-transverse-extension criterion, etc.),
- the transverse in-plane displacements must be interpolated by using the same shape functions as used for the out-of-plane displacements,
- the longitudinal base function for $u(x,y)$ must be the first derivative of the longitudinal base function for $v(x,y)$.
- they must provide $C^{(1)}$ continuous interpolation for the out-of-plane displacements (which is practically useful for defining various end restraints).

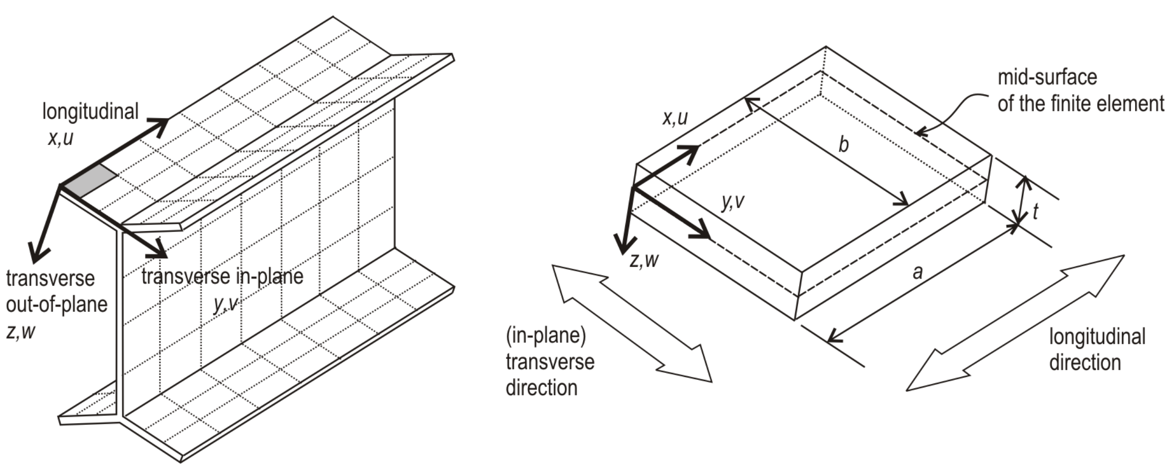

Figure 2: FEM discretization

As one might observe, the distinction of longitudinal and transverse directions is essential. Though unusual in shell finite elements, the element proposed here distinguishes the two perpendicular directions, as illustrated in Fig 2. The proposed interpolation functions are summarized as follows.

$$u(x,y) = \left[N_{y,1}^{(1)} \;\; N_{y,2}^{(1)}\right]\begin{bmatrix}u_1\\u_2\end{bmatrix} \times \left[N_{x,1}^{(2)} \;\; N_{x,2}^{(2)} \;\; N_{x,3}^{(2)}\right]\begin{bmatrix}c_{u1}\\c_{u2}\\c_{u3}\end{bmatrix} \tag{8}$$

$$v(x,y) = \left[N_{y,1}^{(1)} \;\; N_{y,2}^{(1)}\right]\begin{bmatrix}v_1\\v_2\end{bmatrix} \times \left[N_{x,1}^{(3)} \;\; N_{x,2}^{(3)} \;\; N_{x,3}^{(3)} \;\; N_{x,4}^{(3)}\right]\begin{bmatrix}c_{v1}\\c_{v2}\\c_{v3}\\c_{v4}\end{bmatrix} \tag{9}$$

$$w(x,y) = \left[N_{y,1}^{(3)} \;\; N_{y,2}^{(3)} \;\; N_{y,3}^{(3)} \;\; N_{y,4}^{(3)}\right]\begin{bmatrix}w_1\\\Theta_1\\w_2\\\Theta_2\end{bmatrix} \times \left[N_{x,1}^{(3)} \;\; -N_{x,2}^{(3)} \;\; N_{x,3}^{(3)} \;\; -N_{x,4}^{(3)}\right]\begin{bmatrix}c_{w1}\\c_{w2}\\c_{w3}\\c_{w4}\end{bmatrix} \tag{10}$$

where the elementary base functions are given as:

$$N_{x,1}^{(2)} = 1 - \frac{3x}{a} + \frac{2x^2}{a^2} \qquad N_{x,2}^{(2)} = \frac{4x}{a} - \frac{4x^2}{a^2} \qquad N_{x,3}^{(2)} = -\frac{x}{a} + \frac{2x^2}{a^2} \tag{11}$$

$$N_{x,1}^{(3)} = 1 - \frac{3x^2}{a^2} + \frac{2x^3}{a^3} \quad N_{x,2}^{(3)} = x - \frac{2x^2}{a} + \frac{x^3}{a^2} \quad N_{x,3}^{(3)} = \frac{3x^2}{a^2} - \frac{2x^3}{a^3} \quad N_{x,4}^{(3)} = -\frac{x^2}{a} + \frac{x^3}{a^2} \tag{12}$$

$$N_{y,1}^{(1)} = 1 - \frac{y}{b} \qquad N_{y,2}^{(1)} = \frac{y}{b} \tag{13}$$

$$N_{y,1}^{(3)} = 1 - \frac{3y^2}{b^2} + \frac{2y^3}{b^3} \quad N_{y,2}^{(3)} = y - \frac{2y^2}{b} + \frac{y^3}{b^2} \quad N_{y,3}^{(3)} = \frac{3y^2}{b^2} - \frac{2y^3}{b^3} \quad N_{y,4}^{(3)} = -\frac{y^2}{b} + \frac{y^3}{b^2} \tag{14}$$

The above formulae include separate sets of coefficients for the transverse and longitudinal directions. However, these coefficients can easily be exchanged by classic finite element nodal displacements. As an example, the in-plane longitudinal displacement is expressed as follows, see Eq. (8):

$$u(x,y) = \sum_{i=1}^{2}\sum_{j=1}^{3} u_i c_{uj} N_{y,i}^{(1)} N_{x,j}^{(2)} \tag{15}$$

The in-plane longitudinal DOF are the $u_i c_{uj}$ constants, where i=1..2 and j=1..3. Thus, finally, there are 6 such DOF, all of them are translational, and will be denoted here as u_{ij}, as in Fig 3. The interpolation with these finite element DOF:

$$\begin{aligned} u(x,y) = {} & u_{11}N_{y,1}^{(1)}N_{x,1}^{(2)} + u_{13}N_{y,2}^{(1)}N_{x,1}^{(2)} + u_{21}N_{y,1}^{(1)}N_{x,2}^{(2)} + \\ & + u_{23}N_{y,2}^{(1)}N_{x,2}^{(2)} + u_{31}N_{y,1}^{(1)}N_{x,3}^{(2)} + u_{33}N_{y,2}^{(1)}N_{x,3}^{(2)} \end{aligned} \tag{16}$$

Similarly, the in-plane transverse DOF are the $v_i c_{vj}$ constants, see Eq. (9), where i=1..2 and j=1..4. Thus, finally, there are 8 such DOF, which will be denoted here as in Fig 3. Therefore, the v displacement function is interpolated as follows:

$$v(x,y) = v_{11}N_{y,1}^{(1)}N_{x,1}^{(3)} + v_{13}N_{y,2}^{(1)}N_{x,1}^{(3)} + v_{31}N_{y,1}^{(1)}N_{x,3}^{(3)} + v_{33}N_{y,2}^{(1)}N_{x,3}^{(3)} + \\ +\vartheta_{z11}N_{y,1}^{(1)}N_{x,2}^{(3)} + \vartheta_{z13}N_{y,2}^{(1)}N_{x,2}^{(3)} + \vartheta_{z31}N_{y,1}^{(1)}N_{x,4}^{(3)} + \vartheta_{z33}N_{y,2}^{(1)}N_{x,4}^{(3)} \tag{17}$$

The out-of-plane displacement function can be expressed similarly from Eq. (10), by using finite element nodal displacement DOF, as follows:

$$w(x,y) = w_{11}N_{y,1}^{(3)}N_{x,1}^{(3)} + w_{13}N_{y,3}^{(3)}N_{x,1}^{(3)} + w_{31}N_{y,1}^{(3)}N_{x,3}^{(3)} + w_{33}N_{y,3}^{(3)}N_{x,3}^{(3)} + \\ +\vartheta_{x11}N_{y,2}^{(3)}N_{x,1}^{(3)} + \vartheta_{x13}N_{y,4}^{(3)}N_{x,1}^{(3)} + \vartheta_{x31}N_{y,2}^{(3)}N_{x,3}^{(3)} + \vartheta_{x33}N_{y,4}^{(3)}N_{x,3}^{(3)} - \\ -\vartheta_{y11}N_{y,1}^{(3)}N_{x,2}^{(3)} - \vartheta_{y13}N_{y,3}^{(3)}N_{x,2}^{(3)} - \vartheta_{y31}N_{y,1}^{(3)}N_{x,4}^{(3)} - \vartheta_{y33}N_{y,3}^{(3)}N_{x,4}^{(3)} - \\ -\vartheta_{xy11}N_{y,2}^{(3)}N_{x,2}^{(3)} - \vartheta_{xy13}N_{y,4}^{(3)}N_{x,2}^{(3)} - \vartheta_{xy31}N_{y,2}^{(3)}N_{x,4}^{(3)} - \vartheta_{xy33}N_{y,4}^{(3)}N_{x,4}^{(3)} \tag{18}$$

Therefore, the proposed element has 30 DOF: 6 for u, 8 for v. and 16 for w. Each corner node has 7 DOF (1 for u, 2 for v, and 4 for w), while there are two additional nodes at $(x,y)=(a/2,0)$ and $(x,y)=(a/2,b)$ with one DOF per node for the u displacement. The DOF are illustrated in Fig 3.

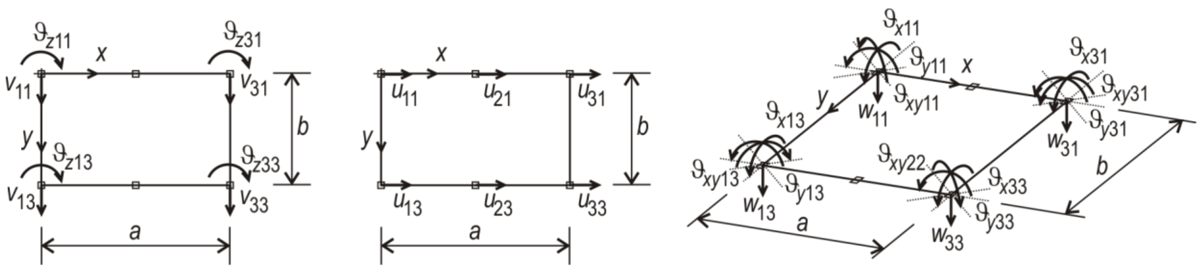

Figure 3: Nodal DOF of the proposed shell finite element

2.3 Constraining

The constraints that are embedded in cFSM are discussed in detail in Ádány and Schafer (2014a,b). It can be observed that the constraints are formulated by setting various displacement derivatives to zero. It can also be observed that the criteria are practically independent of the longitudinal shape functions, therefore, the same criteria can be used for the here-proposed finite element that are used for finite strips. It is also important that the introduction of the mechanical criteria must lead to simple relationships in between the nodal displacement DOF, since this is a necessary condition if the mechanical criteria are intended to be exactly satisfied. The derivation of these relationships (which then are summarized in the **R** constraint matrices) are not given in detail here, but illustrated by a sample. For example, in case of the no-longitudinal-extension criterion, the criterion is

$$\varepsilon_x = \frac{\partial u}{\partial x} = 0 \tag{19}$$

Using the assumed shape functions (with using the notations as in Fig 3), the criterion can be written as:

$$\frac{dN_{x,1}^{(2)}}{dx}\left(u_{11}N_{y,1}^{(1)} + u_{13}N_{y,2}^{(1)}\right) + \frac{dN_{x,2}^{(2)}}{dx}\left(u_{21}N_{y,1}^{(1)} + u_{23}N_{y,2}^{(1)}\right) + \frac{dN_{x,3}^{(2)}}{dx}\left(u_{31}N_{y,1}^{(1)} + u_{33}N_{y,2}^{(1)}\right) = 0 \tag{20}$$

Considering the shape functions and its derivatives, it is easy to conclude that the actual strain function is linear both in *x* and *y*. Therefore, the function can be expressed in the form:

$$C_{11}xy + C_{10}x + C_{01}y + C_{00} = 0 \tag{21}$$

with the *C* coefficients as follows:

$$\begin{gathered} C_{11} = -4(u_{11} - u_{13} - 2u_{21} + 2u_{23} + u_{31} - u_{33})/b/a^2 \\ C_{10} = 4(u_{11} - 2u_{21} + u_{31})/a^2 \\ C_{01} = (3u_{11} - 3u_{13} - 4u_{21} + 4u_{23} + u_{31} - u_{33})/b/a \\ C_{00} = -(3u_{11} - 4u_{21} + u_{31})/a \end{gathered} \tag{22}$$

The longitudinal strain is zero for any *x*-*y* if (and only if) all the *C* coefficients are zero. This is satisfied only if

$$u_{11} = u_{21} = u_{31} \quad \text{and} \quad u_{13} = u_{23} = u_{33} \tag{23}$$

Thus, the no-longitudinal-strain criterion is expressed by the simple relationship in between the nodal degrees of freedom of the proposed shell element. All the other criteria can similarly be handled. Finally, constraint matrices for a single shell element can be formed. Once the elementary constraint matrices are defined, they can be assembled into a global constraint matrix for multiple elements.

2.4 Cross-section modes

In cFSM, if the constraints are applied, specific deformation modes are achieved. These special modes are essentially independent of the member length, which, in other words, means that the deformation modes can be characterized by the deformations of the cross-sections. That is why these special deformation modes are frequently referred as to cross-section modes. In case of the here-proposed cFEM, since the constraining is essentially independent of the longitudinal base functions, the same cross-section modes can be achieved as in cFSM.

It is to highlight that in cFSM/cFEM primary and secondary modes are distinguished. Primary modes are the modes which exist without intermediate nodes within a flat element, while secondary modes the ones that exist only if intermediate nodes are defined. Secondary modes involve zero displacements at the main (corner) nodes and non-zero displacement at the intermediate nodes. G and D modes are primary modes by definition, but local-plate modes have both primary (L_P) and secondary (L_S) sets.

Since in this paper there is a special focus on members with holes, it is important to mention here that in cFSM (as in Ádány and Schafer, 2014a,b) the definition of the modes is independent of the wall thickness of the member (unlike in GBT or in the original version of cFSM). This seemingly small difference has an important practical effect: the cross-section modes are not disturbed by the presence of holes in the member. Therefore, the handling of the holes in the proposed cFSM does not require any special consideration or modification in the method, as well as it does mean any difficulty. cFEM is based on shell FEM, hence, holes are easy to introduce and handle, while the constraining itself is independent of the holes. Thus, though the presence of holes has important effect on the behavior of the member, it has practically no effect on the cFEM calculations.

3. Demonstrative examples

Examples are provided to demonstrate how cFEM works in practice as well as to illustrate its potentials. Since one of the distinguishing feature of cFEM is that it can easily handle holes, the examples will show quite a few cases when holes are present: either a few larger holes, or multiple smaller holes. In all the cases the hole pattern will show certain regularity. It is to emphasize that this regularity of the holes is not a requirement; regular patterns are chosen solely due to the fact that hole patterns tend to be regular in the many practical applications.

For the sake of simplicity, in all the examples the same cross-section is used, which is a lipped channel section with web, flange and lip widths of 200, 80 and 20 mm, respectively. (Note, the dimensions are midline dimensions.) The plate thickness is 2 mm. The member length is 500 mm (which is obviously short for the given case, but using a short member makes it easier to visualize the phenomena). In all the cases the member is supported at its two ends in a globally and locally pinned way. Namely: all the nodes at the end sections are supported perpendicularly to the plates.

As far as loading is concerned, two basic cases are considered. One of the basic case is a simple column problem: the member is in uniform compression, i.e., opposite compressive loads are applied at the end sections, uniformly distributed over the cross-sections. The resultant of the distributed loading is 1 kN.

The other basic case is a bending problem: a transverse concentrated force is applied at the middle of the beam. The action line of the load lays in plane of the web. The value of the loading is 1 kN. Within this basic beam problem three subcases are distinguished depending on the exact position of the load application. If the force is acting at the junction of the web and the top flange, the case is referred as to 'top'. If the force is acting at the junction of the web and the bottom flange, the case is referred as to 'bottom'. Finally, if half of the load is applied at the junction of the top flange, half at the junction of the bottom flange, it will be referred as to "bot-top".

The material is always steel-like. In case of Example 1 the Poisson ratio is set to zero (in order to eliminate the stiffness increasing due to the constraint transverse extension), therefore E=210 000 MPa and G=105 000 MPa are used. In all the other examples standard steel data are assumed: E=210 000 MPa, ν=0.3 and G=80 769 MPa.

3.1 Example 1

Example 1 is the simple column problem. The primary aim of this example is to verify the developed cFEM, by comparing its results to other methods. Critical loads are calculated for various "pure" modes.

In case of global buckling minor-axis buckling, major-axis buckling, pure torsional buckling and flexural-torsional buckling are considered. (Since the lipped channel section is mono-symmetric, major-axis and pure torsional buckling alone do not exist (without some special restraints), but they are combined into flexural-torsional buckling.) The calculated critical values are summarized in Table 1. (Obviously, cFEM provides with multiple eigen-values. Higher values are associated with different wave-lengths. The values shown here are the smallest ones.) To make it possible to compare the results to results of other methods, two options are used, depending on how the second-order effects are taken into consideration. One option is when all the stresses and all the second-order strain terms are considered (which is the obvious option in a shell FE calculation), as in the first row of Table 1. These values are directly comparable to cFSM. Indeed this comparison has been completed, and it was concluded that the differences in between cFEM and cFSM values are negligible (the relative difference being in the order of 10^{-5} or less). In case of the other option only the longitudinal normal stress is considered (which is practically uniform in the whole member), and only the second-order terms of *v* and *w* displacements. This is the parameter setting that imitates the assumptions of the classic beam-model-based critical force formulae, as discussed e.g. in Ádány (2012). By comparing the cFEM results of Table 1 to the classic analytical formulae, again, negligible differences are found.

Table 1: Example 1, critical loads for pure G buckling

stress terms	second-order terms	minor-axis buckling	major-axis buckling	pure torsional buckling	flex-tors buckling
all	all	5872.7	34223	4368.1	4214.9
sig_x only	transverse only	6085.4	42979	4484.4	4323.1

Pure distortional buckling is analyzed, too. Three cases of distortional buckling are considered: symmetrical mode only, point-symmetrical mode only, and both modes. The calculated critical values are summarized in Table 1, while the buckling shapes are shown in Fig 3. As one might expect, when both modes are selected, the first buckling mode is practically identical to the symmetrical case. The results were compared to cFSM results, and practically perfect agreement was found.

Table 2: Example 1, critical loads for pure D buckling

stress terms	second-order terms	symmetric mode	point-symmetric mode	both modes
all	all	250.22	397.43	250.22

Table 3: Example 1, critical loads for pure L buckling

stress terms	second-order terms	primary modes only	primary+10 secondary modes	primary+20 secondary modes
all	all	104.665	77.534	77.530

The results for pure local plate buckling are summarized in Table 3. Three cases are presented here: (a) calculation with the primary L modes only, (b) calculation with the primary modes plus the first 10 secondary L modes, and (c) calculation with the primary modes plus the first 20 secondary L modes. Both the critical values and the deformed shapes clearly show that secondary L modes are non-negligible, but experiences suggest that the first 8-10 secondary modes are enough (unless the first-order solution or the buckling shape includes very small waves). The results can directly be compared to cFSM results, with selecting the wavelengths properly: for the (a) case the wavelength is 500/4=125 mm, while for the (b) and (c) cases the necessary wavelength is 500/3=166.7 mm. Comparison to cFSM, again, shows negligible difference between the cFSM and cFEM results.

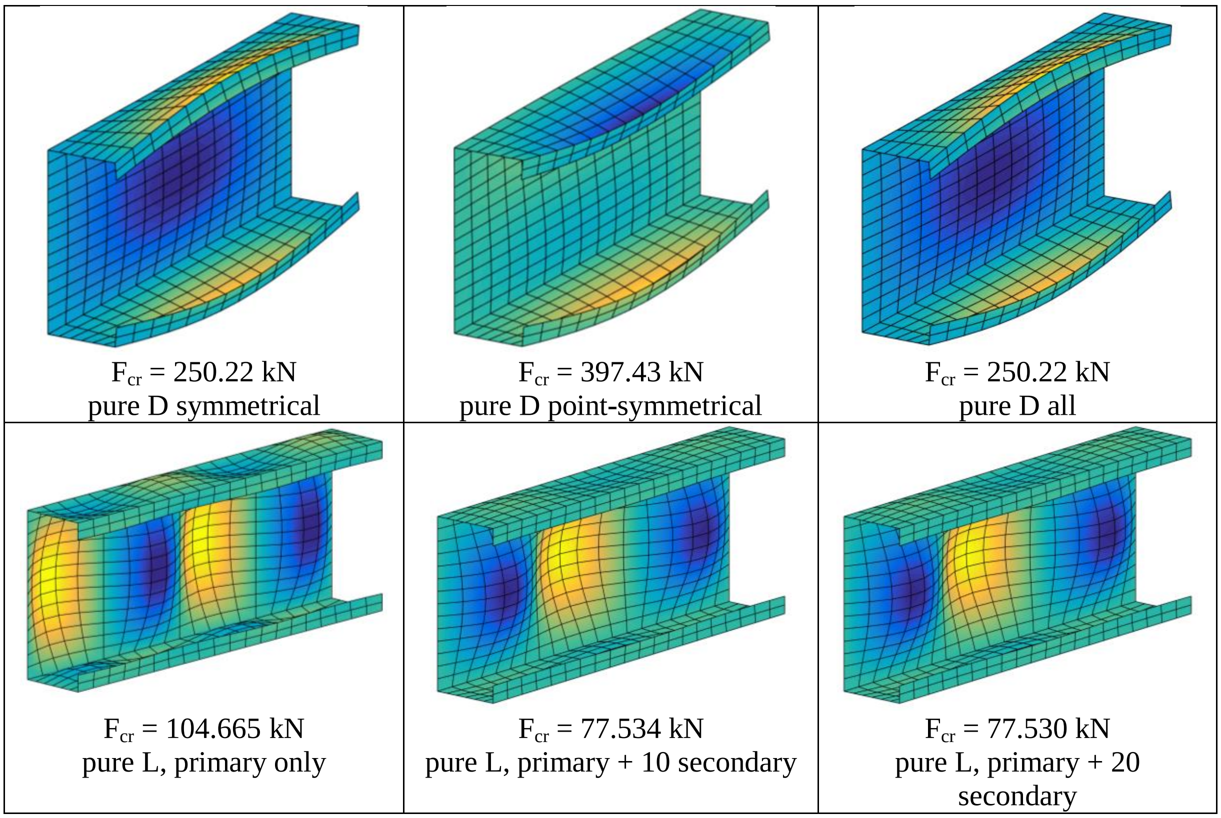

Figure 4: Example 1, buckled shapes for pure D and L modes

From the comparison of basic examples it can be concluded that the proposed cFEM can give practically the same results as analytical solutions or cFSM, if the parameters of the calculations (e.g., restraints, loading, calculation options) are carefully adjusted to those of alternative methods. Another observation is that 8-10 secondary L modes typically enough to use.

3.2 Example 2

Example 2 is the above-described beam problem. Pure G, D and L modes are applied to calculate critical loads. The results are summarized in Table 4, some deformed shapes are shown in Figs 5 and 6. The results highlight that even if the lowest D buckling mode tends to have symmetrical cross-section deformation, the symmetrical and point-symmetrical cross-section modes can combine with each other. The practical consequence is that all the D modes should be selected to have "pure D" buckling solution.

The results clearly show the great importance of the load application point. The general tendency is that the higher the load point, the lower the critical force is. This is well-known for global buckling (i.e., lateral-torsional buckling), but also true for distortional and local-plate buckling. The importance of the load application point can be better understood by looking at the effects of second-order stress terms. It is obvious that the load application point is crucial for the transverse normal stress (i.e. sig_y): when the bottom flange is loaded, the sig_y in the web is mostly tensile, when the upper flange is loaded, the sig_y in the web is mostly compressive, while if the load is equally distributed in between the two flanges, the sig_y in the web is close to zero. Accordingly: if the upper flange is loaded, the most important stress component is the sig_y transverse normal stress. On the other hand: if the lower flange is loaded, the tensile sig_y stress has a stabilizing effect on the buckling due to the combined effect of shear and longitudinal normal stresses.

To have the realistic critical loads ad buckling shapes, there is no reason to disregard any stress component. However, it is useful to switch on and off some stress components in order to better understand the behavior. This might especially be helpful when the stresses are disturbed by the presence of holes.

Table 4: Example 2, critical loads for pure G, D and L buckling

mode	stress terms	bottom	top+bottom	top
G	all	11224	6437.7	3656.5
D sym	all	inf	inf	255.64
D point-sym	all	inf	inf	785.45
D all	all	9934.9	1333.0	245.07
D all	sigx	3384.6	2882.4	2491.5
D all	sigy	180508	883.51	229.37
D all	tauxy	2446.3	2955.7	2964.4
L	all	127.08	70.681	35.403
L	sigx	136.91	142.76	139.66
L	sigy	778.59	95.137	34.699
L	tauxy	86.916	101.59	104.15

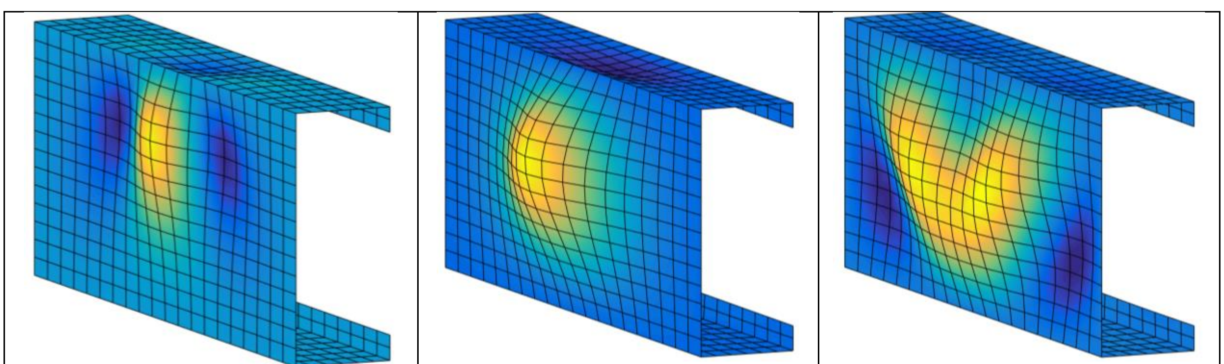

F_{cr} = 139.66 kN
L, sig_x, top

F_{cr} = 34.699 kN
L, sig_y, top

F_{cr} = 104.15 kN
L, tau_xy, top

Figure 5: Example 2, buckled shapes for pure L modes due to various stress components

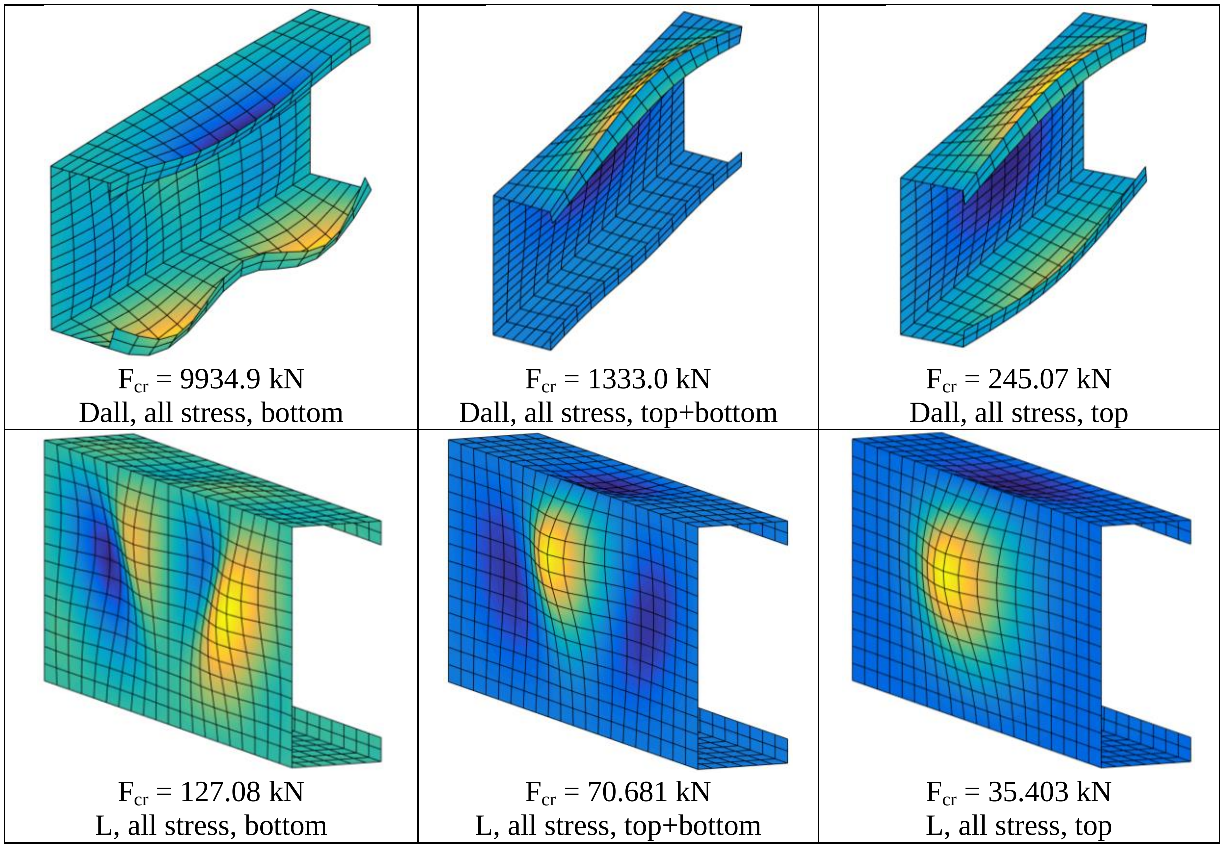

Figure 6: Example 2, buckled shapes for pure D and L modes

3.3 Example 3

Example 3 is the above-described beam problem (as in Example 2), but in the web there is a centrally placed square hole of varying size (50mm, 100mm, 150mm). The calculated critical forces are given in Table 5, where the no-hole cases are also included for the sake of comparison. Some selected buckled shapes are shown in Figs 7 and 8.

Table 5: Example 3, critical loads for pure G, D and L buckling

mode	hole dimension	bottom	top+bottom	top
G	no	11224	6437.7	3656.5
D	no	9934.9	1333.0	245.07
L	no	127.08	70.681	35.403
G	50	10872	6323.0	3644.9
D	50	10810	1332.4	240.64
L	50	122.03	66.902	31.979
G	100	9664.3	5885.0	3548.8
D	100	14578	1412.4	231.33
L	100	98.293	60.036	27.188
G	150	7627.2	4997.8	3217.7
D	150	6769.9	1468.7	215.57
L	150	47.803	55.900	22.140

As one might expect, the presence of the hole usually decreases the critical force: the larger the hole, the more important the degradation. However, this tendency is not always true: a smaller size centrally placed hole might increase the critical force value, as demonstrated by the pure D critical values. The phenomenon can be explained by the stress distribution: even though the stiffness is degraded due to the hole, the stress distribution might favorably be changed, and in some cases the stress distribution effect might be the more important one. As the buckled shapes show, the presence of the hole might considerably change the way how the beam buckles.

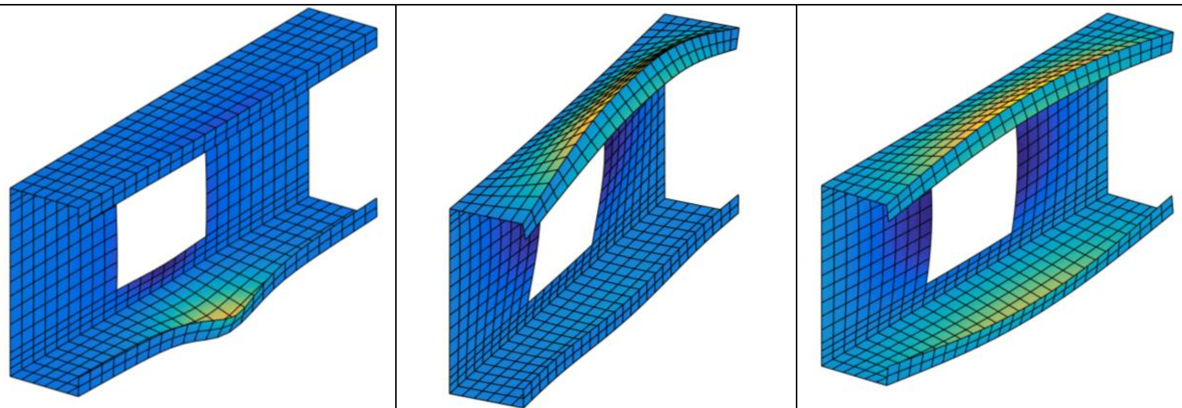

F_{cr} = 6769.9 kN D, 150mm hole, bottom	F_{cr} = 1468.7 kN D, 150mm hole, top+bottom	F_{cr} = 215.57 kN D, 150mm hole, top

Figure 7: Example 3, buckled shapes for pure D modes

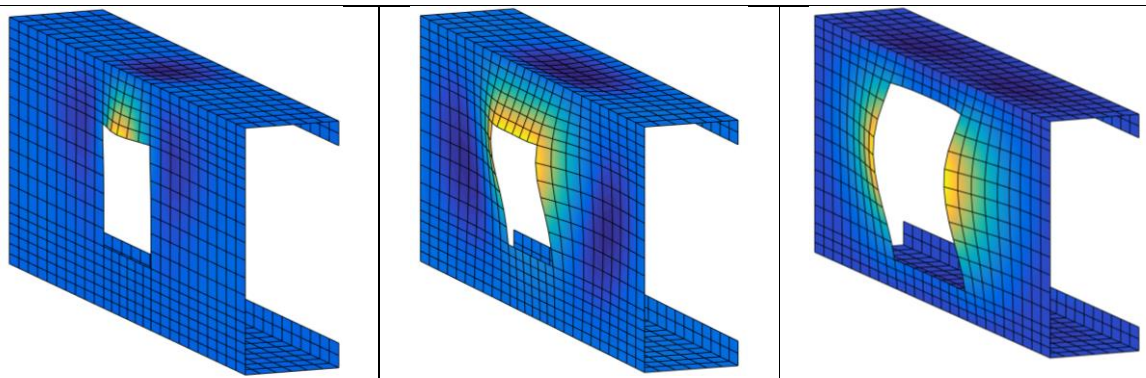

F_{cr} = 98.293 kN L, 100mm hole, bottom	F_{cr} = 60.036 kN L, 100mm hole, top+bottom	F_{cr} = 22.140 kN L, 150mm hole, top	D, 150mm

Figure 8: Example 3, buckled shapes for pure L modes

3.4 Example 4

Example 4 is the above-described beam problem (as in Example 2), but with a square hole of 100mm size. The position of the hole is central in between the flanges, but changing along the length, the middle point of the hole being 100mm, 150mm, 200mm and 250mm from the beam end. (Note, when the position is 250mm, the hole is centrally placed, see Example 3.) The results are summarized in Table 6 and Fig 9.

Table 6: Example 4, critical loads for pure G, D and L buckling

mode	hole position	bottom	top+bottom	top
G	100	25656	8484.2	2236.3
D	100	7290.4	2328.6	719.91
L	100	21.053	3.4599	1.3018
G	150	24023	7711.0	2081.6
D	150	8657.1	2814.1	345.06
L	150	8.9425	4.9303	1.6819
G	200	15538	6788.0	2742.5
D	200	22377	3417.4	292.49
L	200	63.893	12.597	2.1786
G	250	9664.3	5885.0	3548.8
D	250	14578	1412.4	231.33
L	250	98.293	60.036	27.188

The effect of the hole position is quite dependent on the buckling mode and on the load position. In case of global buckling, the critical force is increasing as the hole moves toward the end of the beam. In case of local buckling the tendency is (mostly) the opposite. In fact, the L critical force is drastically reduced if the hole is near the beam end. In case of distortional buckling the tendency is also dependent on the load position. If the top flange is loaded, the critical force is increasing as the hole moves toward the beam end, however, in other cases the highest critical forces are calculated when the hole is somewhere in between the middle and the end of the beam.

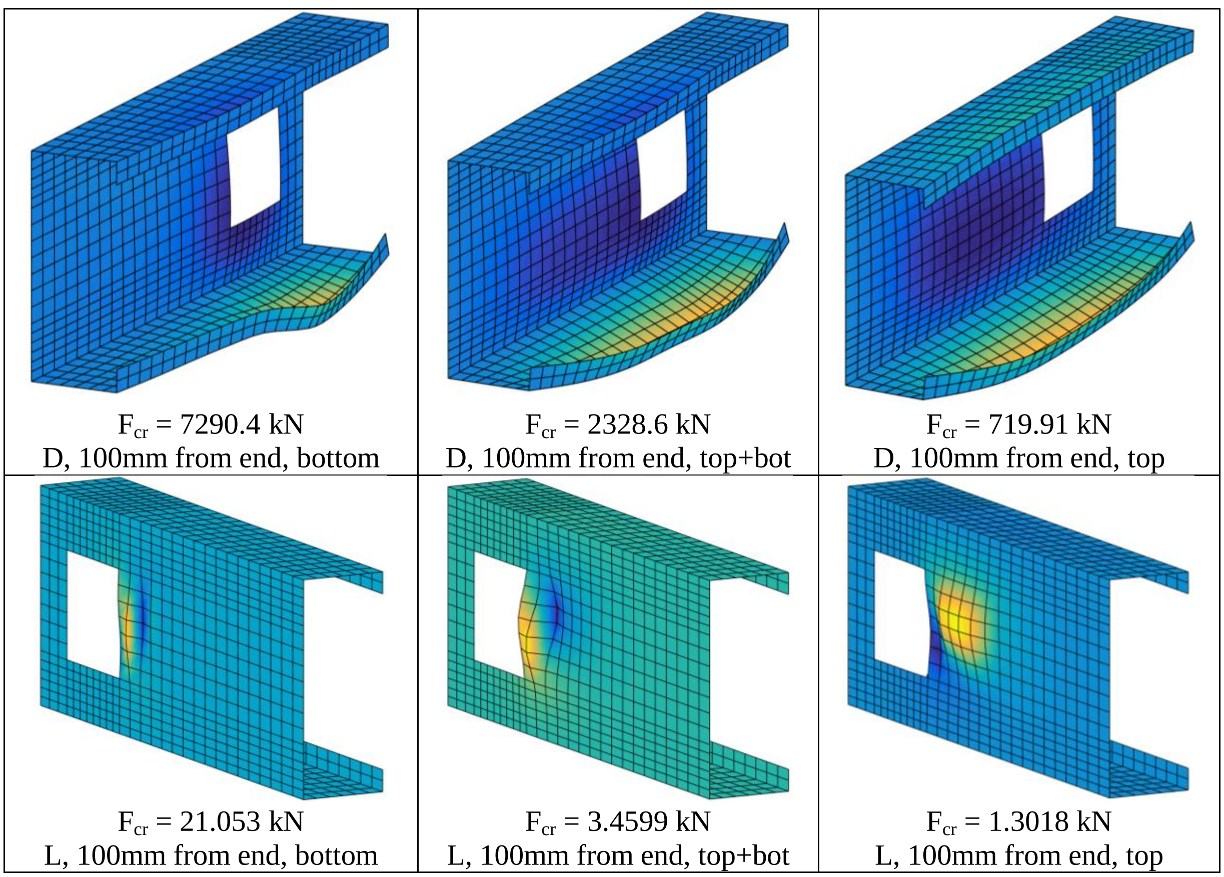

Figure 9: Example 4, buckled shapes for pure D and L modes

3.5 Example 5

Example 5 is the above-described beam problem (as in Example 2), but with multiple slot rows in the middle of the web. Two cases are presented here: 3 slot rows and 11 slot rows. The results are given in Table 7 and in Figs 10 and 11.

The tendency for global buckling is simple: the more slot rows we have, the smaller the critical forces are. In case of local and distortional buckling, if the lower flange is loaded, the introduction of more and more slot rows decreases the critical force values. However, if the upper flange is loaded, the slot rows increase the L and D critical forces. This seemingly strange tendency can clearly be explained by the sig_y stresses. Since sig_y can hardly develop due to the slots, they can hardly stabilize the L/D buckling when the lower flange is loaded, but they have less degrading effect when the upper flange is loaded (compared to the solid web case).

Table 7: Example 5, critical loads for pure G, D and L buckling

mode	slot rows	bottom	top+bottom	top
G	no	11224	6437.7	3656.5
D	no	9934.9	1333.0	245.07
L	no	127.08	70.681	35.403
G	3	11598	6414.7	3449.8
D	3	3342.7	2351.9	486.51
L	3	48.574	100.97	59.226
G	11	11578	6245.7	3183.3
D	11	863.28	1030.4	955.11
L	11	21.692	47.931	73.466

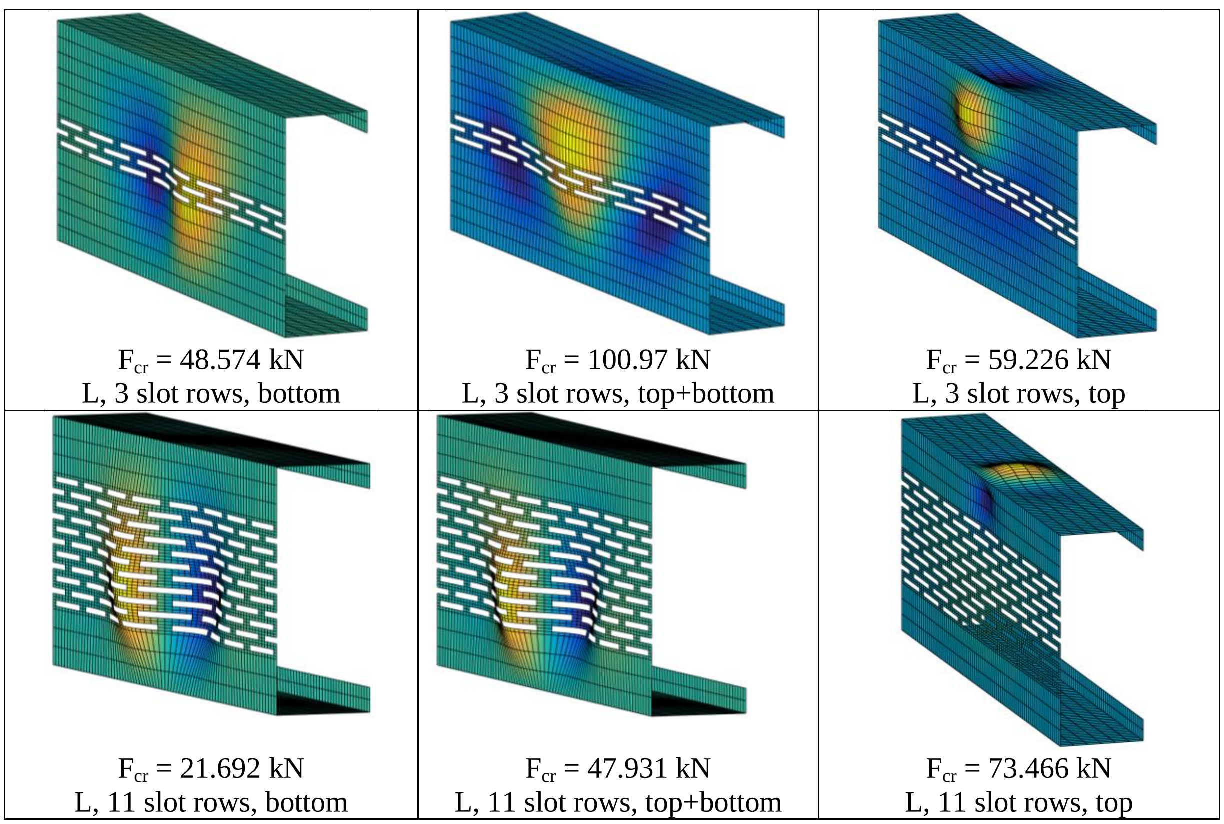

Figure 10: Example 5, buckled shapes for pure L modes

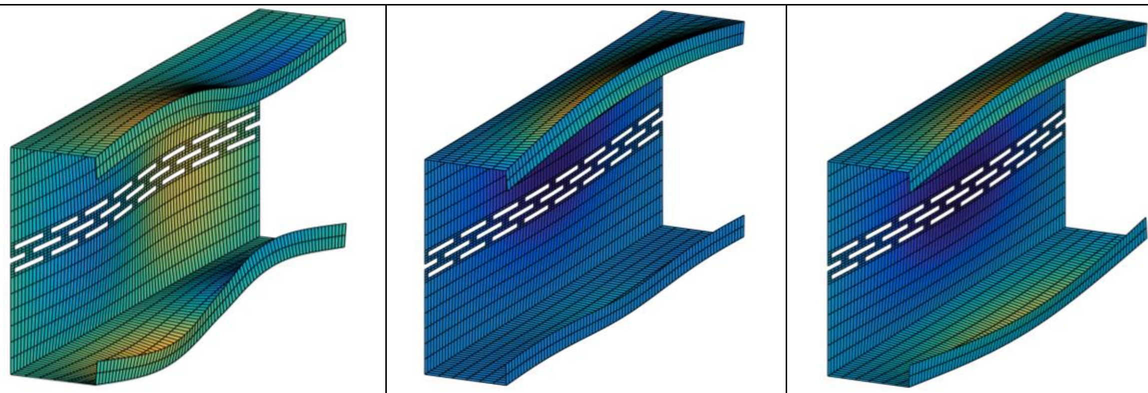

F_{cr} = 3342.7 kN D, 3 slot rows, bottom	F_{cr} = 2351.9 kN D, 3 slot rows, top+bottom	F_{cr} = 486.51 kN D, 3 slot rows, top

Figure 11: Example 5, buckled shapes for pure D modes

3.6 Example 6

Example 6 is similar to Example 2, but with multiple square holes of various sizes and arranged in various patterns. Four patterns are presented here, as shown in Figs 12 and 13. The critical force values are summarized in Table 8.

The examples demonstrate that the cFEM can handle practically arbitrary hole pattern, provided the pattern can well be modeled by using a rectangular finite element mesh. If there is large number of small holes, obviously, a fine mesh is necessary, which means longer calculation time.

As the results to various hole patterns demonstrate, the behavior can be significantly influenced by the presence of the holes. Though there are exceptions, the tendency is that the stiffness reduction caused by the holes is dominant, therefore, usually the introduction of holes decreases the critical forces.

Table 8: Example 6, critical loads for pure G, D and L buckling

mode	hole pattern	bottom	top+bottom	top
G	no	11224	6437.7	3656.5
D	no	9934.9	1333.0	245.07
L	no	127.08	70.681	35.403
G	a	9168.4	5445.1	3171.1
D	a	2637.5	1031.1	225.92
L	a	31.613	31.241	14.636
G	b	10781	6278.1	3618.5
D	b	8403.6	1907.8	248.46
L	b	80.106	71.084	32.564
G	c	10041	5822.6	3341.3
D	c	8028.7	1982.2	248.59
L	c	85.561	60.750	30.814
G	d	10696	6209.6	3567.6
D	d	9918.7	1685.1	245.64
L	d	117.18	75.634	32.717

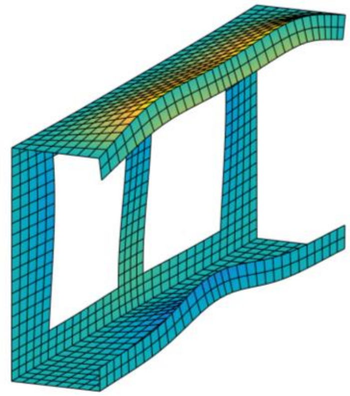 F_{cr} = 2637.5 kN D, pattern a, bottom	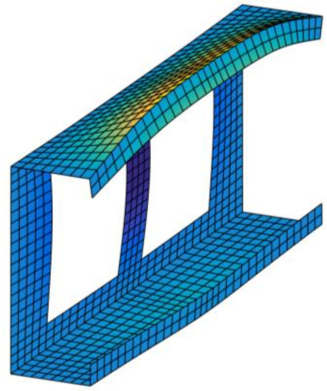 F_{cr} = 1031.1 kN D, pattern a, top+bottom	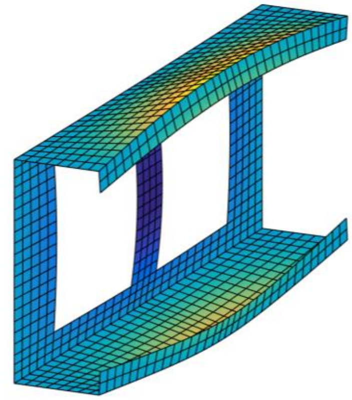 F_{cr} = 225.92 kN D, pattern a, top
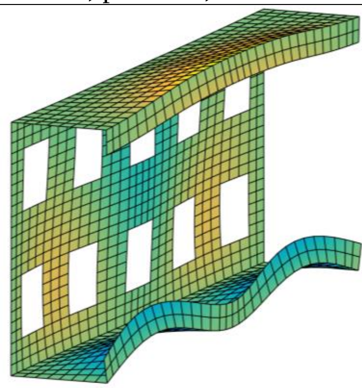 F_{cr} = 8028.7 kN D, pattern c, bottom	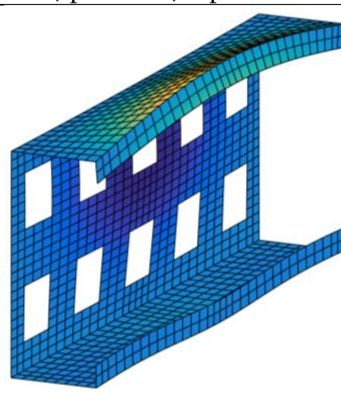 F_{cr} = 1982.2 kN D, pattern c, top+bottom	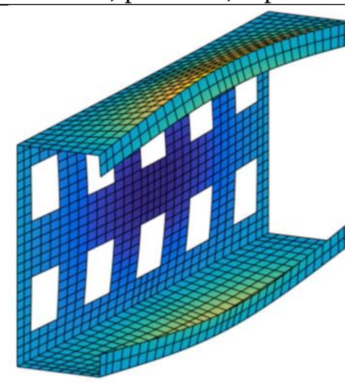 F_{cr} = 248.59 kN D, pattern c, top
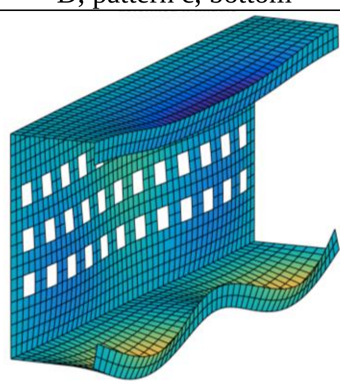 F_{cr} = 9918.7 kN D, pattern d, bottom	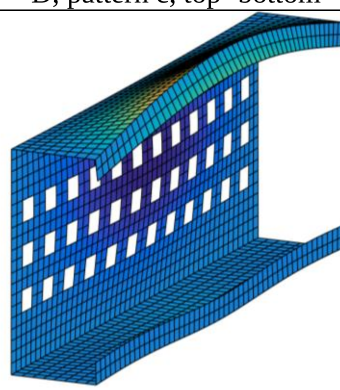 F_{cr} = 1685.1 kN D, pattern d, top+bottom	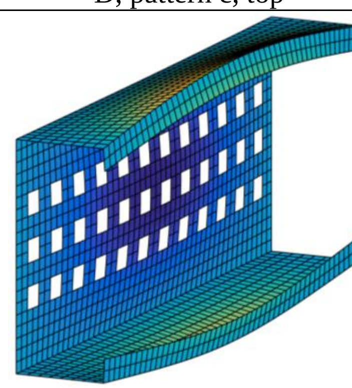 F_{cr} = 245.64 kN D, pattern d, top

Figure 12: Example 6, buckled shapes for pure D modes

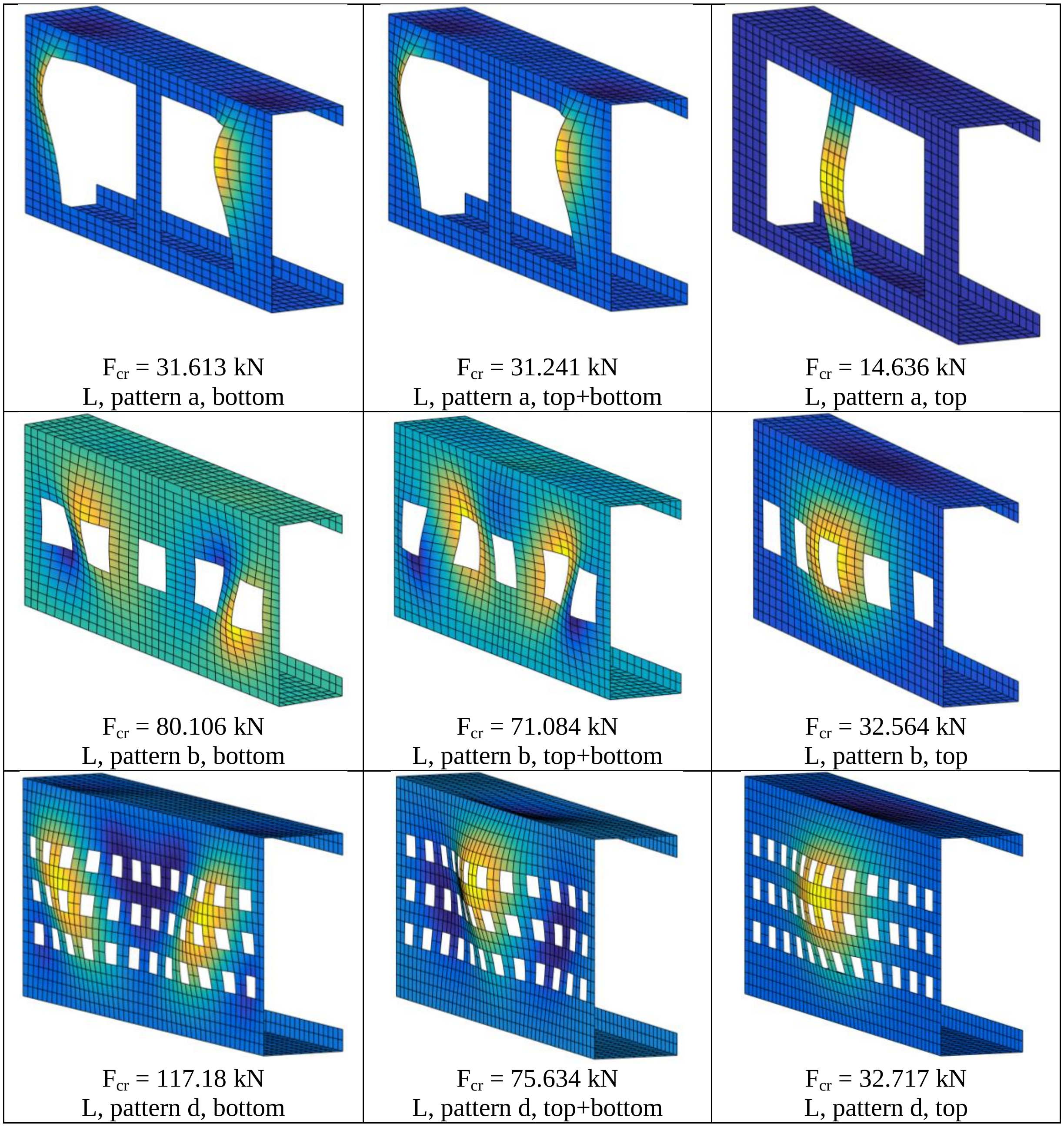

Figure 13: Example 6, buckled shapes for pure L modes

3.7 Example 7

Example 7 is similar to Example 2, but with a centrally placed oval hole. The diameters of the hola are 160mm and 120mm longitudinally and transversally, respectively. The results are summarized in Table 9 and in Fig 14. Due to the fact that the developed cFEM requires a rectangular mesh, the oval hole can be modelled only approximately. Still, it is reasonable to assume that the results are good approximations of the precise ones. Obviously, finer mesh might lead to better approximation. From the results it can be concluded that the behavior and tendencies are similar (though not identical) to those of Example 3 (where one centrally placed square hole is introduced).

Table 9: Example 7, critical loads for pure G, D and L buckling

mode	hole	bottom	top+bottom	top
G	no	11224	6437.7	3656.5
D	no	9934.9	1333.0	245.07
L	no	127.08	70.681	35.403
G	160×120 oval	8936.8	5670.5	3559.0
D	160×120 oval	18101	1295.8	212.93
L	160×120 oval	96.407	53.863	23.780

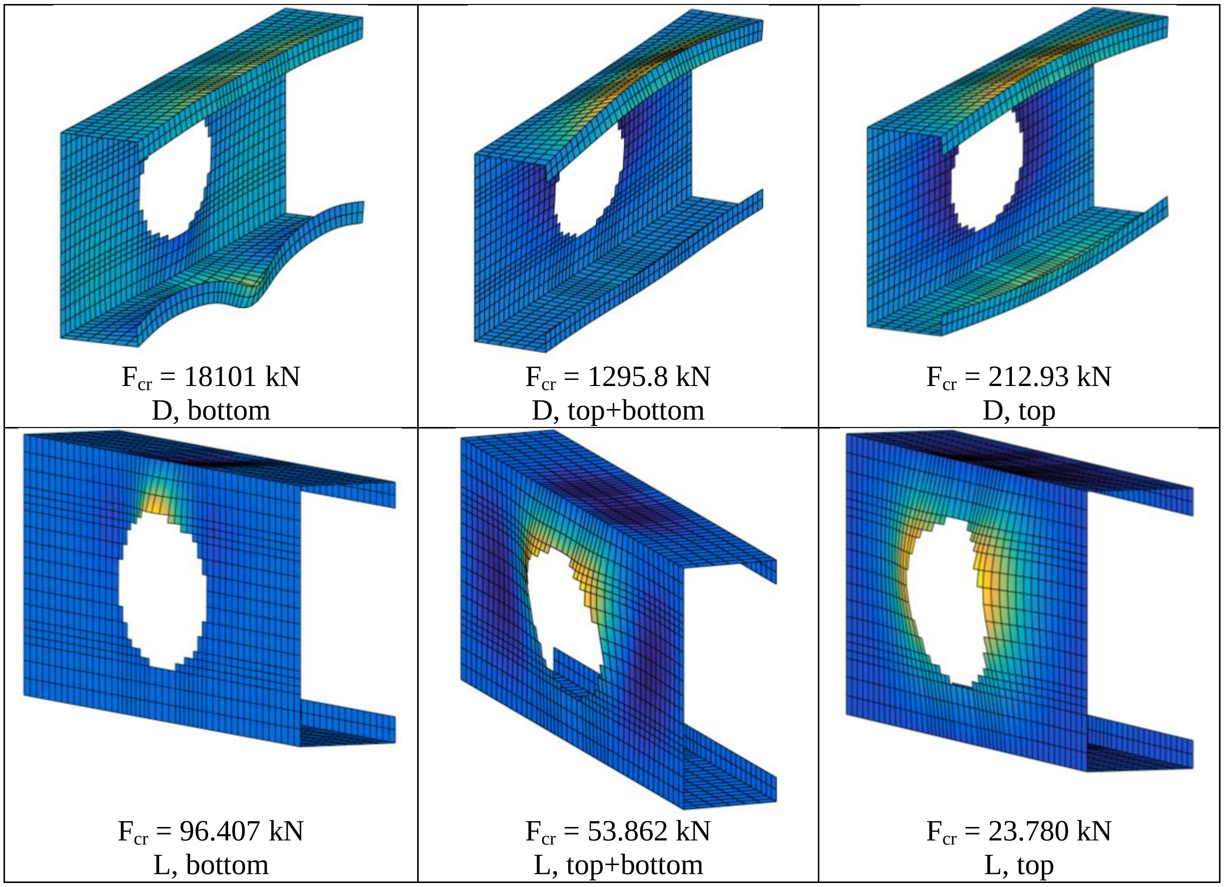

F_{cr} = 18101 kN
D, bottom

F_{cr} = 1295.8 kN
D, top+bottom

F_{cr} = 212.93 kN
D, top

F_{cr} = 96.407 kN
L, bottom

F_{cr} = 53.862 kN
L, top+bottom

F_{cr} = 23.780 kN
L, top

Figure 14: Example 7, buckled shapes for pure D and L modes

4. Conclusions

In this paper a novel method is introduced for the modal decomposition of the deformations of thin-walled members. The method applies essentially the same constraining technique as the constrained finite strip method, however, the member is discretized both in the transverse and longitudinal directions, and the longitudinal base functions are modified accordingly: from the trigonometric functions of FSM to polynomial functions that are widely used in the finite element method. Due to these changes, the new method can readily be described as constraint finite element method, which possesses the same modal features as the constrained finite strip method, but with significantly extended practical applicability. The new method requires a highly regular mesh, but otherwise it can handle arbitrary restraints and loading, can easily handle members with holes, can handle some cross-section changes, and potentially can further be extended to many other applications (e.g., frames, etc.).

The applicability of the proposed method is demonstrated by multiple numerical examples in the paper. A special focus is on the presence of holes. As the numerical examples proves, the method can easily handles the holes in practically arbitrary arrangements. The numerical examples also illustrate the complex behavior caused by the holes. It is believed that the newly proposed method will be a useful tool to better understand the behavior of thin-walled members, as well as to extend the modal decomposition technique to areas not explored yet.

Acknowledgments

The work was conducted with the financial support of the OTKA K108912 project of the Hungarian Scientific Research Fund.

References

Ádány S. (2012). Global Buckling of Thin-Walled Columns: Analytical Solutions based on Shell Model, *Thin-Walled Structures*, Vol 55, pp 64-75.

Ádány, S., Schafer, B.W. (2006a). Buckling mode decomposition of single-branched open cross-section members via Finite Strip Method: derivation, *Thin-Walled Structures* **44**(5), pp. 563-584.

Ádány, S., Schafer, B.W. (2006b). Buckling mode decomposition of single-branched open cross-section members via Finite Strip Method: application and examples, *Thin-Walled Structures*, **44**(5), pp. 585-600.

Ádány, S., Schafer, B.W. (2008). A full modal decomposition of thin-walled, single-branched open cross-section members via the constrained finite strip method, *Journal of Constructional Steel Research*, 64 (1), pp. 12-29..

Ádány S., Schafer B.W. (2014a). Generalized constrained finite strip method for thin-walled members with arbitrary cross-section: Primary modes, *Thin-Walled Structures*, Vol 84, pp. 150-169.

Ádány S., Schafer B.W. (2014b). Generalized constrained finite strip method for thin-walled members with arbitrary cross-section: Secondary modes, orthogonality, examples, *Thin-Walled Structures*, Vol 84, pp. 123-133.

Cai J., Moen C.D. (2015). Generalized beam theory buckling analysis for members with holes, Eighth International Conference on Advances in Steel Structures, Lisbon, Portugal, July 22-24, 2015, paper no:86, p. 18.

Casafont M., Marimon F., Pastor M.M., Ferrer M. (2011). Linear buckling analysis of thin-walled members combining the Generalised Beam Theory and the Finite Element Method, *Computers and Structures*, 89(21-22), Nov 2011, pp. 1982-2000.

Casafont M., Bonada J., Pastor M.M. and Roure F. (2015). GBT calculation of distortional and global buckling of cold-formed steel channel columns with multiple perforations, Eighth International Conference on Advances in Steel Structures, Lisbon, Portugal, July 22-24, 2015, paper no:87, p. 18.

Cheung, Y.K. (1976). Finite strip method in structural analysis, Pergamon Press, 1976.

Eccher, G., Rasmussen, K.J.R. Zandonini, R. (2009). Geometric nonlinear isoparametric spline finite strip analysis of perforated thin-walled structures, Thin-Walled Structures, Volume 47, Issue 2, February 2009, Pages 219-232.

Hancock, G.J. (1978). Local, Distortional, and lateral buckling of I-beams, ASCE *Journal of structural engineering*, 104(11), pp. 1787-1798.

Li, Z., Schafer B.W. (2009). Finite Strip Stability Solutions for General Boundary Conditions and the Extension of the Constrained Finite Strip Method, in *Trends in Civil and Structural Engineering Computing*. 2009. Stirlingshire, UK: Saxe-Coburg Publications.

Li, Z., Schafer, B.W. (2010). Buckling analysis of cold-formed steel members with general boundary conditions using CUFSM: Conventional and constrained finite strip methods, *Proceedings* of the 20th International Specialty Conference on Cold-Formed Steel Structures - Recent Research and Developments in Cold-Formed Steel Design and Construction, p. 17.

Silvestre N., Camotim D., Silva N.F. (2011). Generalized Beam Theory revisited: from the kinematical assumptions to the deformation mode determination, *Int. Journal of Structural Stability and Dynamics*, 11(5), Oct 2011, pp. 969-997.